

ORIGINAL ARTICLE

# Evolution of Inflammation and White Matter Injury in a Model of Transient Focal Ischemia

Iska Moxon-Emre, BSc and Lyanne C. Schlichter, BSc, MSc, PhD

## Abstract

After an ischemic stroke, there is a prolonged inflammatory response and secondary phase of injury that is more amenable to treatment than acute neurotoxicity. Surprisingly, little is known about temporal and spatial relationships between inflammation and white matter injury. Here, we quantified development of white matter damage, inflammation, and a *glial limitans* at 1, 3, and 7 days after transient ischemia in the rat striatum using immunohistochemistry. Quantitative analysis showed that decreased staining for myelin basic protein and increased staining for damaged myelin basic protein began in the core, coincided with neutrophil infiltration, and progressed outward over time. Axon damage (i.e. accumulation of amyloid precursor protein) began at the edge of the lesion, coinciding with substantial microglia/macrophage activation, and progressed into the core. During the 7 days, activated microglia/macrophages dramatically increased only in the core and edge of the lesion. Detailed spatial analyses revealed that activated microglia/macrophages that surrounded undamaged axon bundles did not express ED1, a marker of phagocytic cells, whereas those inside damaged bundles expressed ED1. These results imply different contributions of neutrophils and microglia/macrophages to white matter injury after ischemic stroke. The distinct localizations of activated microglia/macrophages imply complex signals that regulate their migration toward and infiltration of damaged white matter.

**Key Words:** Axonal injury, Brain ischemia, Endothelin-1, Glial limitans, Microglia/Macrophage activation, Myelin damage, Neutrophils, Stroke.

## INTRODUCTION

Thromboembolic stroke leads to ischemic brain injury, and the resulting loss of brain cells is a leading cause of death and long-term disability (1, 2); thus, many experimental stroke studies have focused on neuron death. Initially, white matter was thought to be resistant to stroke, but it is now recognized that axons and myelin are susceptible to hypoxic and excito-

toxic insults (3–5). White matter damage disrupts normal neuronal transmission and thus likely is a key predictor of the outcome (6–8).

After an ischemic stroke, there is a secondary injury phase that can progress for hours to days, with the development of a penumbra in which neurons and white matter are at risk (9–13). This phase is characterized by a prominent inflammatory response that is delayed in onset and is thus temporally more amenable to treatment than acute neurotoxicity (14–16). Neutrophils, microglia, and macrophages are assumed to contribute to secondary neuronal damage, but the role of microglia is widely debated because of their capacity to produce both cytotoxic mediators and molecules that can aid in damage resolution and repair (17–19). It has been postulated that white matter is particularly vulnerable to inflammatory mediators (20), and that inflammation after stroke might damage white matter at times and in locations in which no loss of neurons is seen. Surprisingly, very few studies have examined the coevolution of inflammation and white matter damage after stroke (5, 21). There are little or no quantitative data concerning temporal and spatial relationships between inflammatory cells (i.e. neutrophils, microglia, macrophages) and axon and myelin damage. Moreover, there are discrepancies in the published data, even when the same model was used.

Approximately 25% of ischemic infarcts in humans are lacunar and result from occlusion of small perforating arteries that supply subcortical regions of the brain; these infarcts usually affect deep cerebral white matter and basal ganglia (22, 23). To model this form of transient focal ischemic stroke, we injected the vasoconstrictor peptide, endothelin-1, into the rat striatum (5, 21, 24–26). This method produced a reproducible lesion that was restricted to the anterior striatum (i.e. caudate plus putamen) and was surrounded by relatively normal striatal tissue. We used this model to quantify the temporal and spatial progression of damage to myelin and axons, and its relationship to neutrophils, activated microglia, and macrophages.

## MATERIALS AND METHODS

### Induction of Transient Focal Cerebral Ischemia and Tissue Preparation

All procedures were approved by the University Health Network Animal Care Committee in accordance with guidelines established by the Canadian Council on Animal Care. Adult male Sprague-Dawley rats (250–350 g, 3–4 months old)

From the Toronto Western Research Institute, University Health Network, and Department of Physiology, University of Toronto, Toronto, Canada.

Send correspondence and reprint requests to: Lyanne C. Schlichter, BSc, MSc, PhD, Toronto Western Hospital, 399 Bathurst St, MC 9-415, Toronto, Ontario, Canada M5T 2S8; E-mail: schlicht@uhnres.utoronto.ca

This work was supported by operating grants HSFO, T5546, and T6279 from the Heart & Stroke Foundation of Canada, Ontario Chapter to Lyanne C. Schlichter. Iska Moxon-Emre received a Frederick Banting and Charles Best Canada Graduate Scholarship from the Canadian Institutes for Health Research.

were anesthetized and placed in a small-animal stereotaxic instrument (David Kopf Instruments, Tujunga, CA). Under aseptic conditions, skin coverings were cleared, and a 1-mm-diameter burr hole was drilled in the skull (0.2 mm anterior and 3.5 mm lateral to bregma) and a 30-gauge needle was then lowered into the right caudate putamen (6 mm ventral to the skull surface). The vasoconstrictor peptide, endothelin-1 (Calbiochem, EMD Biosciences, Gibbstown, NJ), was injected to produce transient focal ischemia (5, 24–27). During a 5-minute period, 400 pmol endothelin-1 in 1  $\mu$ L PBS was injected using an UltraMicroPump II (World Precision Instruments, Sarasota, FL). The needle was left in place for a further 5 minutes to prevent solution reflux. Control animals ( $n = 9$ ) were injected with 1  $\mu$ L saline. Each animal's core body temperature was maintained at 36.5°C using an electric heating pad throughout surgery and recovery. No rats died as a result of the surgery. We used the minimum number of animals necessary for statistical analysis of a large number of parameters. All endothelin-1-injected rats ( $n = 12$ ) displayed behavioral deficits (e.g. ipsilateral turning bias) but were able to eat, drink, and groom themselves. This protocol produced a lesion in part of the striatum with a surrounding zone of relatively undamaged tissue for comparison. An earlier study using endothelin-1 showed that reducing local blood flow in the striatum and cortex by more than 60% produced a lesion of about the same size (5).

Animals were killed at 1, 3, or 7 days by an overdose of the anesthetic isoflurane. For staining with 2,3,5-triphenyl-2H-tetrazolium chloride ([TTC] Sigma-Aldrich, St Louis, MO) to determine the lesion volume, rats were perfused transcardially with 60 mL PBS (pH 7.5). The brains were removed, cut at 2 and 10 mm from the anterior end using a brain matrix, and 500- $\mu$ m-thick sequential slices were made with a VT 1000S vibratome (Leica, Richmond Hill, Ontario, Canada). The 16 serial sections were incubated in 2% TTC for 30 minutes in a 37°C water bath, photographed with a digital camera, and analyzed with ImageJ software (version 1.33 k, National Institutes of Health). For immunohistochemistry, they were perfused with 4% paraformaldehyde (EMD Biosciences) and 2% sucrose in PBS (pH 7.5). The isolated brains were stored in the same fixative at 4°C for 24 hours, then in 10% sucrose for 24 hours, and finally in 30% sucrose until they were sectioned. Coronal slices were made at 3, 6, and 9 mm from the anterior end of the brain. Frozen brain sections (16  $\mu$ m thick) were made using a cryostat (Model CM350S, Leica) and stored at -40°C until used.

### Immunohistochemistry

Individual brain sections were circled with a PAP pen and then incubated overnight at 4°C in PBS containing 3% normal donkey serum, 0.3% Triton X-100, and the appropriate primary antibody, as follows. Mouse monoclonal anti-MBP (1:100; Sigma-Aldrich) was used to detect MBP (Fig. 1A). Regions of myelin damage or demyelination were identified with a rabbit polyclonal antibody that recognizes only degraded MBP ([dMBP] 1:250; Chemicon, Temecula, CA) (28). Accumulation of amyloid precursor protein (APP) was detected with rabbit polyclonal anti-APP (1:250; Zymed, South San Francisco, CA). Neutrophils were labeled with rabbit polyclonal anti-myeloperoxidase (1:50; Dako-Canada,

Mississauga, Canada). Astrocytes were labeled with mouse monoclonal anti-glial fibrillary acidic protein ([anti-GFAP] 1:500; Sigma-Aldrich). Microglia/macrophages were labeled with rabbit polyclonal anti-ionized calcium-binding adapter-1 ([anti-Iba1] 1:1000; Wako, Japan). Mouse monoclonal anti-ED1 (1:100; Serotec, Raleigh, NC) was used to label the lysosomes of highly activated phagocytic microglia/macrophages. For secondary antibody labeling, the sections were washed in PBS (3 $\times$ , 10 minutes each) and then incubated (2 hours, room temperature) in PBS containing 3% normal donkey serum, 0.3% Triton X-100, and both a Cy3-conjugated donkey anti-rabbit antibody and a fluorescein isothiocyanate-conjugated donkey anti-mouse antibody. The sections were washed twice in PBS (10 minutes each), and then 4'-6-diamidino-2-phenylindole (DAPI) (1:5000 Sigma-Aldrich) was applied for 5 minutes, followed by another 10-minute wash in PBS. Negative controls were treated in the same manner but omitting the primary antibody.

The slides were coverslipped using 50:50 glycerol-PBS and examined with an LSM 510 META confocal fluorescence microscope (Zeiss, Oberkochen, Germany). To reduce variability in staining intensity, all immunohistochemistry was carried out on the same day for each stain with the same reagents; ipsilateral and contralateral hemispheres of each animal were compared. For intensity and area analysis, all images were captured using the same pinhole size, intensity, and contrast settings, and with short exposure times at low (5 $\times$  or 10 $\times$ ) magnification to prevent fading. As a further validation, no evidence of fading (decreased intensity) was seen when 10 consecutive images were taken from the same location.

### Quantifying Myelin and Axonal Damage, Immune Cells, and the Astrocytic Response

Before performing detailed analyses, we validated an unbiased sampling procedure and assessed whether the needle entry and fluid injection caused damage. The ipsilateral striatum of control saline-injected animals ( $n = 9$ ) was compared with the contralateral striatum for the key parameters that were to be quantified (Fig. 1C). To validate the unbiased sampling procedure, we tested for differences in densities of microglia/macrophages (Iba1-labeled cells) at 3 locations along the rostral-caudal axis with respect to the injection site (1 mm anterior, center, 1 mm posterior) at each of the experimental time points (1, 3, 7 days) as follows. For each ipsilateral section from endothelin-1-injected animals, 4 200  $\times$  200- $\mu$ m areas were assessed in each of 3 regions: the core, edge of the infarct, and surrounding striatum (a total of 12 sample areas from each of the 3 locations along the rostral-caudal axis). In the undamaged contralateral striatum of endothelin-1-treated animals, 4 larger sampling areas (369  $\times$  369  $\mu$ m) were assessed at the 3 locations along the rostral-caudal axis; regional details were not needed because there was no lesion. Quantitative analysis (2-way analysis of variance [ANOVA]) showed that there were no statistical differences in densities of microglia/macrophages (Iba1-labeled cells) along the rostral-caudal axis (data not shown), providing further evidence against fluid injection-mediated damage.

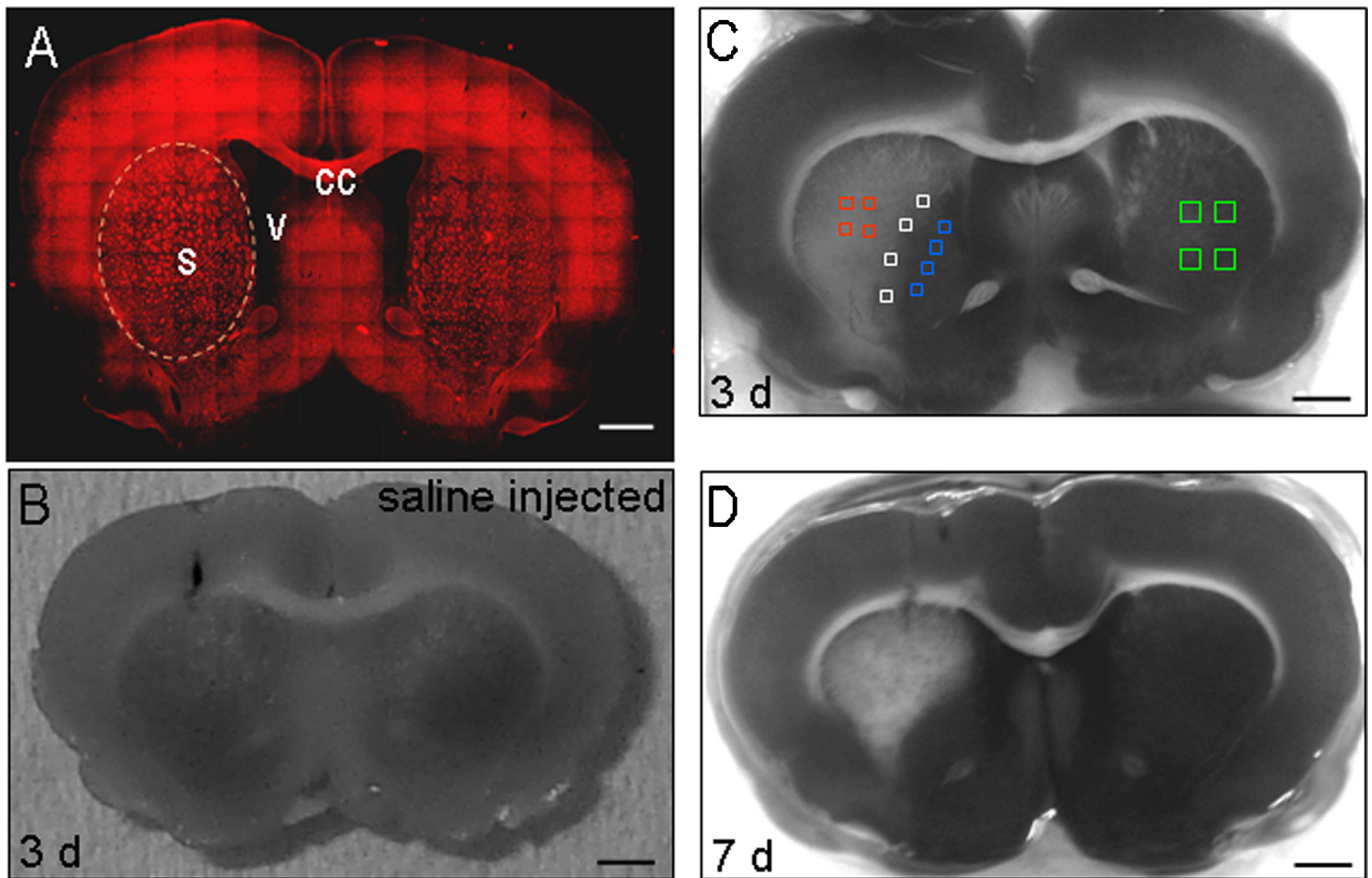


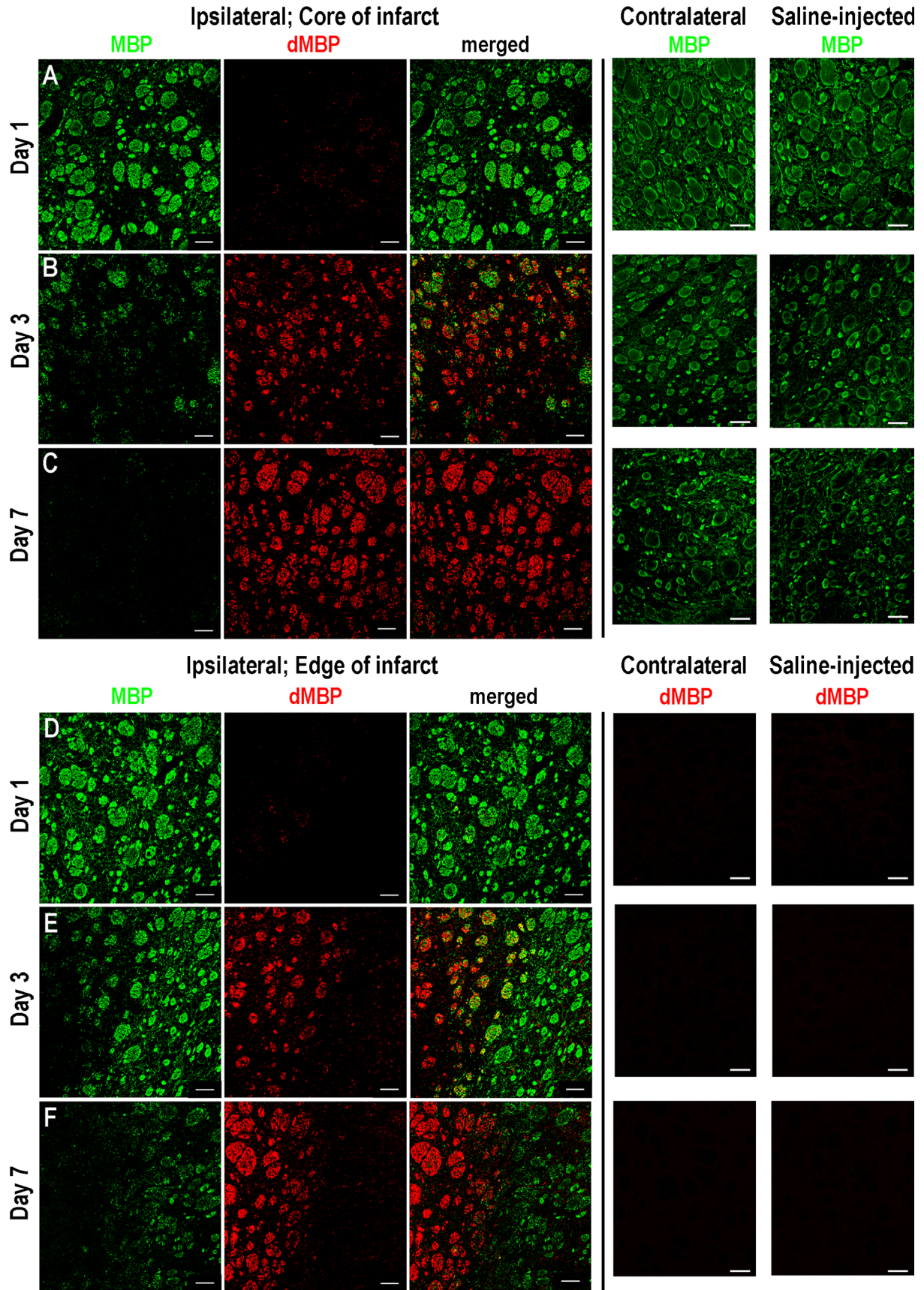
**FIGURE 1.** Stroke model and sampling procedure. **(A)** Coronal section of normal rat brain (+2 mm from anterior) stained for myelin basic protein. Note the structure of the striatum (S) with approximately circular myelinated axon bundles seen in cross section. **(B)** Saline injection (1  $\mu$ L) into the striatum did not produce an infarct, as shown in a coronal section at 3 days, stained with 2% TTC. The needle entry tract is visible on the left. **(C, D)** Transient focal ischemia was induced in the rat striatum by injecting 400 pmol of endothelin-1 in 1  $\mu$ L saline. Representative coronal sections at 3 days **(C)** and 7 days **(D)**, stained with 2% TTC. Panel C illustrates the unbiased counting procedure; 4  $200 \times 200$ - $\mu$ m sampling areas each were analyzed in the core of the infarct (red boxes), at the edge of the infarct (white boxes), and in the surrounding ipsilateral striatum (blue boxes) and compared with 4 ( $369 \times 369$   $\mu$ m) sampling areas in the undamaged contralateral striatum (green boxes). Scale bars = 1 mm. CC, corpus callosum; V, lateral ventricle.

After this validation of sampling procedures, all subsequent analyses of cell densities, staining areas, and intensities used 1 brain section from the center of the injection site, then averaged multiple sample areas from each location, and compared the ipsilateral and contralateral sides. The sample areas had different sizes depending on the parameter assessed. White matter tracts vary in diameter and density throughout the striatum. Therefore, to reduce this variability when quantifying MBP and dMBP at each region, 2 large ( $500 \times 500$   $\mu$ m) sampling areas were analyzed for each section. Staining intensities were quantified by subtracting the background fluorescence, converting the images to a gray scale and then calculating the mean gray value using ImageJ software. For the same sample sites, the area fraction of staining was calculated by ImageJ after the background fluorescence was subtracted. The area of APP staining was quantified using the same method except that comparison of the undamaged contralateral striatum was omitted because there was no detectable APP staining. For analyzing the astrocytic response, GFAP-stained areas and

intensities were quantified in 4  $200 \times 200$ - $\mu$ m sampling areas each, from the core, edge of infarct, and surrounding striatum (12 areas per brain section) and compared with the 4 larger sampling areas ( $369 \times 369$   $\mu$ m) from the undamaged contralateral striatum. This approach was more accurate than counting cells because it accounts for the increase in GFAP immunostaining in reactive astrocytes (29) and avoids inaccuracies resulting from their complex morphology. The densities of microglia/macrophages (anti-Iba1 or anti-ED1) were counted in 4  $200 \times 200$ - $\mu$ m sampling areas each from the core, edge of infarct, and surrounding striatum (12 areas per brain section), and compared with 4 larger sampling areas ( $369 \times 369$   $\mu$ m) from the undamaged contralateral striatum.

### Statistical Analysis

Staining intensities in the damaged regions (core, edge of infarct) were normalized to the undamaged contralateral striatum of the same animal, which was set to 1.0 for MBP and GFAP and 0 for dMBP. For each analysis, mean values



within a zone (core, edge of infarct, contralateral striatum) were first obtained for the number of preselected sampling areas for each stain. The data are presented as mean  $\pm$  SEM (except for Fig. 8E) for the number of animals indicated. Differences were determined by 1-way ANOVA or 2-way ANOVA when assessing 2 independent variables: time and brain region. In both instances, ANOVA was followed by the Bonferroni correction; differences were considered significant if  $p < 0.05$ .

## RESULTS

### Temporal and Spatial Relationships Between Myelin Loss and Damage to Myelin and Axons

The striatum is well delineated and penetrated by white matter bundles (Fig. 1A). This feature facilitated a detailed spatial analysis of the relationship between inflammation and white matter damage and allowed us to compare staining with multiple antibodies at the same site. Metabolically compromised regions show pale staining with TTC. Injecting saline (1  $\mu$ L) did not cause damage, as shown by TTC staining at 3 days (Fig. 1B) and by control immunostaining in several later figures. In contrast, large infarcts were evident at 3 and 7 days after endothelin-1 injection (Figs. 1C, D). The unbiased counting procedure is illustrated in Figure 1C. Staining with TTC was also used at 3 days to demonstrate the reproducibility of the endothelin-1 model. The infarct volume was measured in sequential 500- $\mu$ m-thick slices through the entire lesion in a cohort of animals ( $n = 6$ ). The mean total volume at 3 days was  $41 \pm 2$  mm<sup>3</sup>.

The progression of myelin damage was monitored using antibodies against MBP and dMBP (28) at 1, 3, and 7 days after the stroke. Figure 2 shows representative confocal images in the core and at the lesion edge, from the contralateral striatum, and from the injection site center for saline-injected rats. Staining with MBP was very similar in saline-injected controls to that in the undamaged contralateral side (Figs. 2A–C, right panels), and there was no dMBP staining (Figs. 2D–F, right panels). Thus, for subsequent quantitative analysis, we compared the damaged ipsilateral to the undamaged contralateral striatum of each rat. Comparing staining in the same animal was useful for reducing any variability in antibody labeling and imaging. Figure 3 shows quantification of the mean intensity and fraction of total area stained compared with the undamaged contralateral striatum. The  $p$  values are explained in the figure legends because several statistical comparisons were made on each graph. At Day 1, MBP staining in the core of the infarct appeared normal (Fig. 2A), and the staining intensity and area fraction did not differ from the contralateral striatum (Figs. 3A, B). Staining for dMBP was restricted to small puncta in the core (Fig. 2A), which was reflected by an increase in mean dMBP intensity (Fig. 3C) but not in the area fraction (Fig. 3D). From Days 1 to 7, there was a progressive loss in intensity (Fig. 3A) and area fraction (Fig. 3B) of MBP

staining in both the core and at the edge of the infarct (Fig. 2). During the same time course, there was a progressive increase in damaged myelin in the core and at the edge; the intensity (Fig. 3C) and area (Fig. 3D) of dMBP staining increased. Damage in the core was more severe than at the edge, and there was a clear delineation between the 2 regions (Figs. 2E, F).

In healthy CNS neurons, APP is present throughout axons and fast anterograde transport maintains a low concentration that is difficult to detect by immunohistochemistry. When this transport fails, APP accumulates, and it is thus a useful marker of axonal damage (30, 31) and detects more subtle damage than routine histopathologic stains (32). There was no evidence of axonal damage in the undamaged contralateral striatum or in saline-injected animals (Figs. 4A–C, right panels). By Day 1 in the ipsilateral striatum, there was very little APP staining at the edge of the infarct but a small increase in the core (Figs. 4A, D). This corresponds well with a lack of change in MBP staining at this time (Figs. 2A, D; 3A, B). From Days 3 to 7, APP staining increased first at the edge of the infarct and then in the core after a delay (Fig. 4D). On Day 3, there was punctate APP staining inside myelinated bundles at the edge (Fig. 4B). Similar spatial comparisons could not be made for the core and at Day 7 because of the extensive loss of MBP staining (Figs. 2B, C, F, 3A, B).

### Formation of a Glial Limitans

On Day 1, there was a decrease in both GFAP staining intensity (Fig. 5D) and fractional area occupied (Fig. 5E) within the core, but normal-appearing astrocytes were present at the edge of the infarct (Figs. 5A, D, E). By Day 3, many astrocytes displayed a reactive phenotype with shorter processes and increased GFAP staining intensity, and an astrocytic boundary had developed (Fig. 5B) that remained on Day 7 (Fig. 5C). From Days 1 to 7, both the intensity (Fig. 5D) and area (Fig. 5E) of GFAP staining increased at the edge of the infarct and decreased in the core.

On Day 1, Iba1-labeled microglia with processes were distributed throughout the core and edge of the lesion (Fig. 5A). On Days 3 and 7, the core was filled with intensely stained macrophages/microglia (Figs. 5B, C). By Day 7, this resulted in a clear boundary between intense GFAP and Iba1 staining at the edge of the infarct (Fig. 5C). We use the collective term *microglia/macrophages* for the rounded-up cells (Figs. 6B, C) because activated microglia with retracted processes are indistinguishable from macrophages (33).

The distribution of Iba1 staining was compared with highly activated (likely phagocytic) microglia/macrophages labeled with an antibody against the lysosomal marker, ED1. At all times examined, the density of Iba1-labeled cells outside the lesion was the same as in the undamaged contralateral striatum (Fig. 6D), and ED1-positive cells were not detected (Figs. 6A–C, left side in each ED1 image). Progressively staining with Iba1 and ED1 increased in the core and at the

**FIGURE 2.** Temporal and spatial changes in normal and damaged myelin. **(A–C)** Core of the infarct. Representative confocal images of sections double labeled for normal myelin (anti-myelin basic protein [MBP], green) and damaged myelin ([dMBP] red) at 1, 3, and 7 days after stroke induction. **(D–F)** Edge of the infarct showing representative confocal images of double-labeled sections, as in **(A–C)**. The core is out of view to the left. The pairs of panels to the right compare the contralateral striatum with saline-injected rats per time point. Scale bars = 100  $\mu$ m.

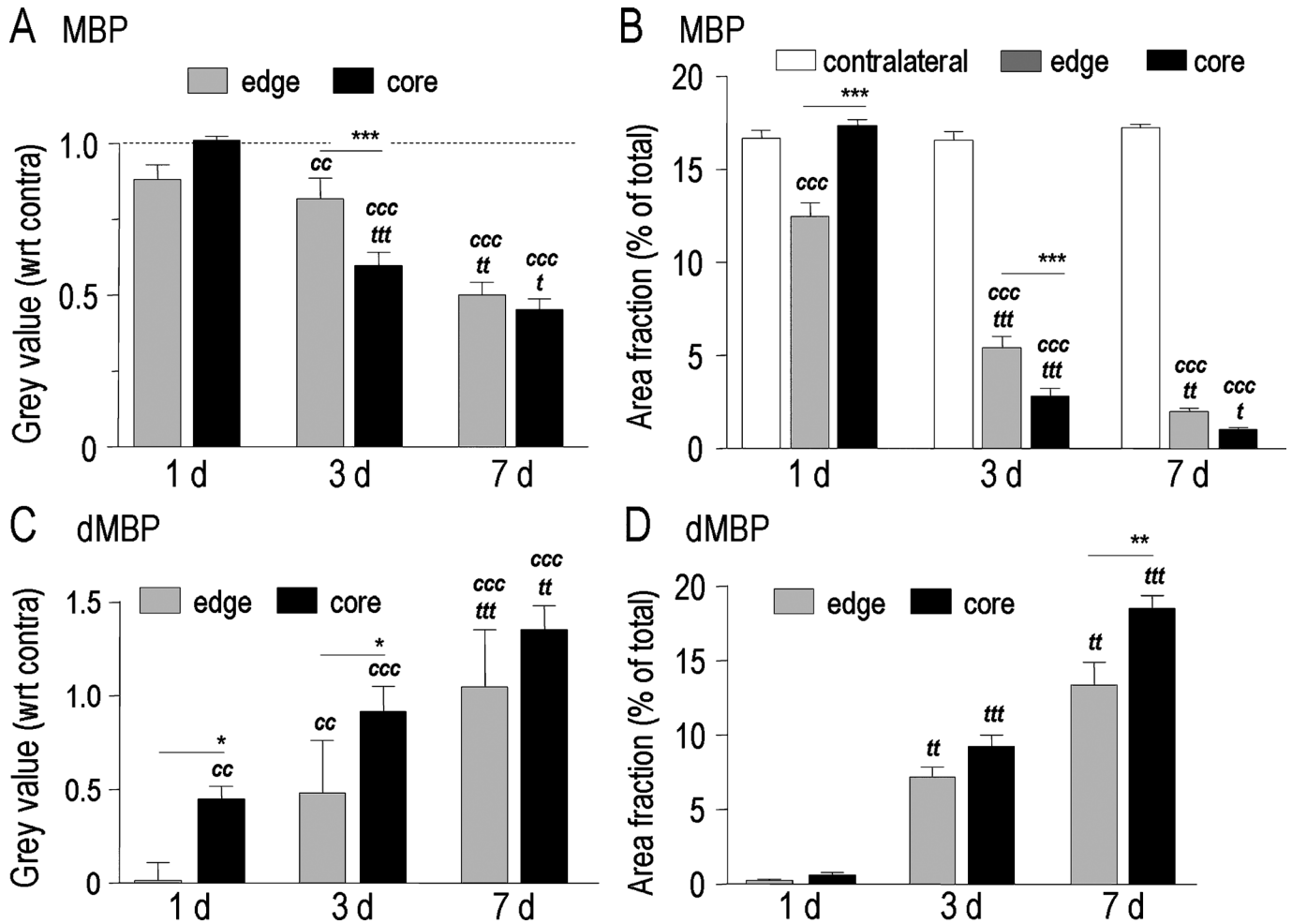


**FIGURE 3.** Quantification of the loss of normal myelin and increase in damaged myelin. Summary of the temporal and spatial changes in intensity (normalized to the contralateral striatum; dotted line) and area of staining (expressed as percent of total area examined) from 1 to 7 days after an ischemic stroke. Values are shown as mean  $\pm$  SEM for  $2\,500 \times 500\text{-}\mu\text{m}$  sampling areas at each location and time (4 rats per time point). Statistical comparisons are based on 2-way analysis of variance with Bonferroni post hoc tests. Levels of significance are indicated as follows: 1 symbol of any type,  $p < 0.05$ ; 2 symbols,  $p < 0.01$ ; 3 symbols,  $p < 0.001$ . The different symbols refer to the following comparisons: *c*, differences from the contralateral striatum; *t*, differences from the previous time point at the same site; \* differences between adjacent values marked with a horizontal bar, that is, core versus edge. **(A, B)** Myelin basic protein (MBP). The staining intensities in the core and at the edge of the infarct were compared with the contralateral side, which was set to 1.0 (dotted line). The area of staining in each location (core, edge, undamaged contralateral striatum) is expressed as a percent of the total area analyzed. **(C, D)** Damaged MBP (dMBP). The staining intensity was compared as in **(A)** but with staining on the contralateral side set to 0 (i.e. after the very low background fluorescence was subtracted). The percentages of area stained were calculated as in **(B)**, but only the core and edge were analyzed because there was no dMBP staining on the undamaged contralateral side.

edge of the infarct (Figs. 6D, E), but the density of ED1-stained cells was always lower than of Iba1-stained cells (Figs. 6F, G), with about 50% as many ED1-positive cells on Days 3 and 7. Differential staining is seen in higher magnification images (Figs. 6B, C, right panels), in which arrowheads indicate examples of cells stained with Iba1 but not ED1.

### General Spatial and Temporal Relationship Between Inflammation and Myelin Damage

We next assessed whether neutrophils that rapidly infiltrate after stroke (34–36) correspond temporally and spatially

with myelin damage. On Day 1, many neutrophils (i.e. small round myeloperoxidase-stained cells) were present inside and around the myelinated bundles in the core (Fig. 7A). Thereafter, the numbers of neutrophils progressively decreased, and by Day 3, most remaining neutrophils were outside the myelinated bundles. This observation is important because by Day 3, the MBP staining had decreased (Figs. 2A, B, 7B), and most bundles contained dMBP (Fig. 2B). By Day 7, neutrophils and normal MBP staining were not detected in the core (Fig. 7C), whereas all bundles contained dMBP (Fig. 2C). There was a different temporal and spatial relationship between myelin damage and Iba1-positive microglia/macrophages (37). There

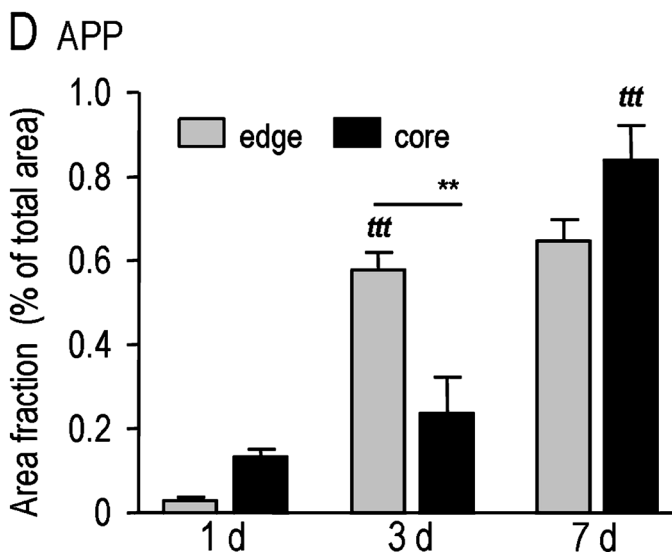
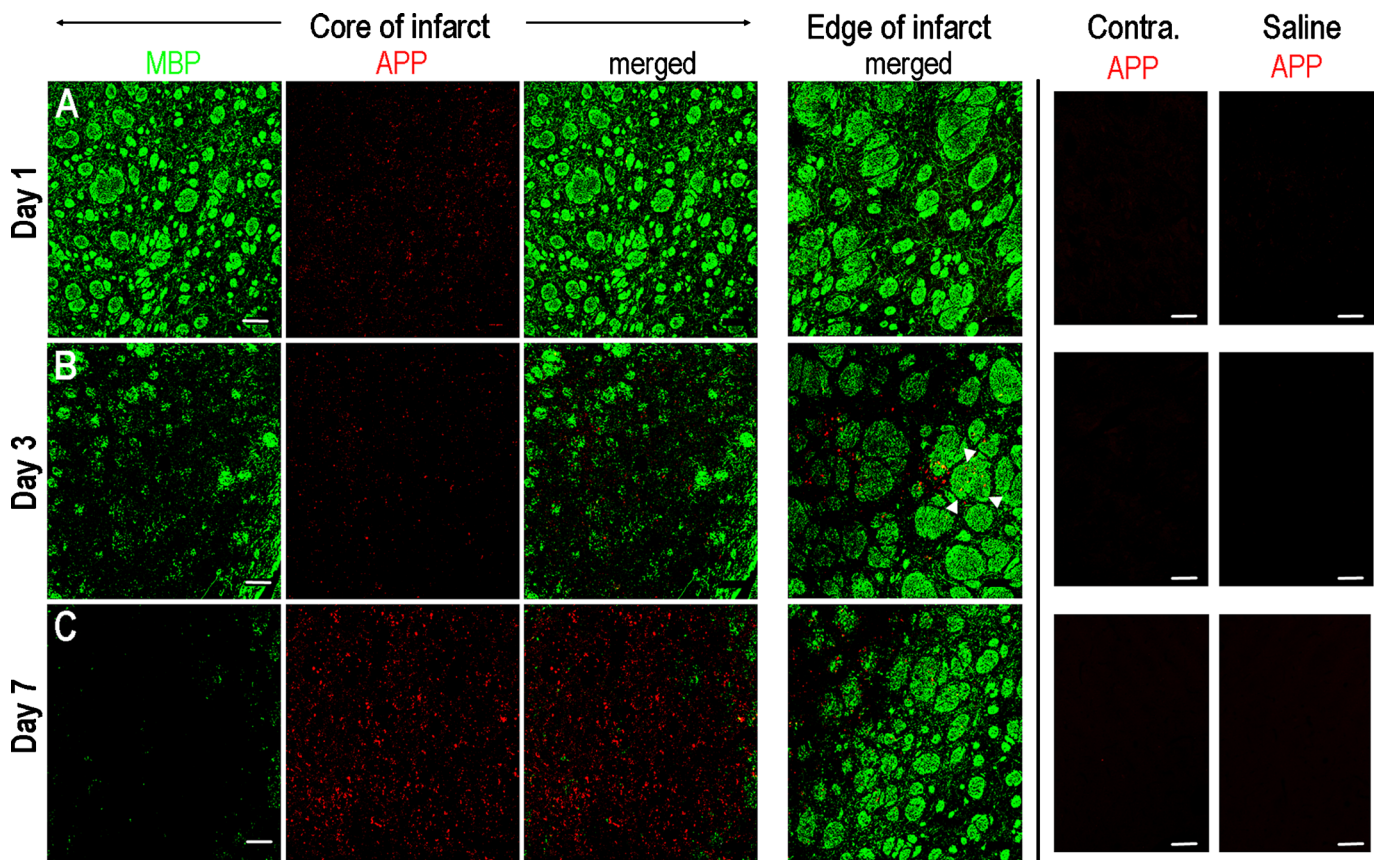


**FIGURE 4.** Temporal and spatial analysis of axonal damage. Accumulation of amyloid precursor protein (APP) was monitored with a rabbit polyclonal anti-APP antibody (red) and compared with staining for normal myelin using a mouse monoclonal anti-myelin basic protein ([MBP] green). **(A–C)** Representative confocal images of sections double labeled for MBP and APP in the core of the infarct (left panels). The center is out of view to the left. In the merged images from the edge of the infarct (right panels), arrowheads surround a myelinated bundle containing puncta of APP staining. The pairs of panels to the right compare the contralateral striatum with saline-injected rats per time point. Scale bars = 100  $\mu$ m. **(D)** Summary of changes in the area fraction (expressed as percent of total area examined) for APP staining in the core and at the edge of the infarct from 1 to 7 days after the stroke. Values are shown as mean  $\pm$  SEM for 2 500  $\times$  500- $\mu$ m sampling areas at each location and time (4 rats per time point). Statistical comparisons are based on 2-way analysis of variance with Bonferroni post hoc tests.

was relatively weak Iba1 staining of ramified microglia in the undamaged contralateral striatum at each time point (Fig. 7). In control saline-injected animals, some microglia were more brightly stained with larger cell bodies at Day 1 (resolved by Day 3), but if this reflected transient microglial activation, it

did not cause white matter damage, as judged by the lack of dMBP and APP staining at 3 and 7 days. In the ipsilateral striatum on Day 1, microglia/macrophages with retracted processes were prevalent between but not inside the myelinated bundles in the core and at the edge of the infarct

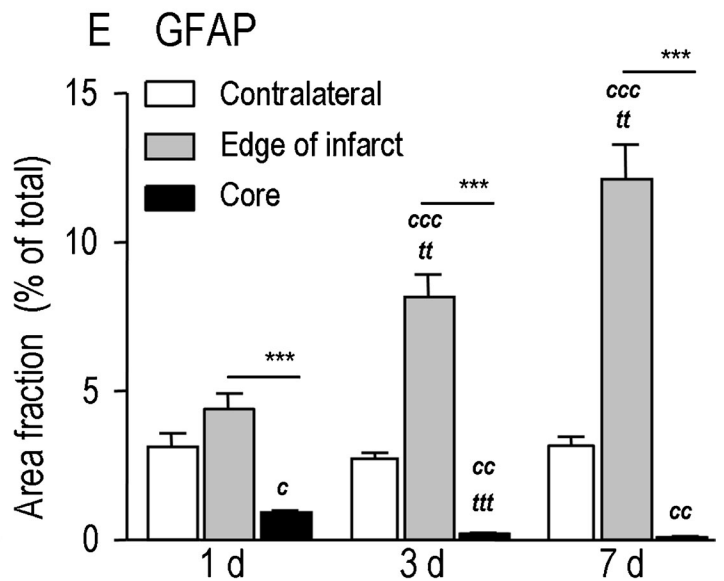
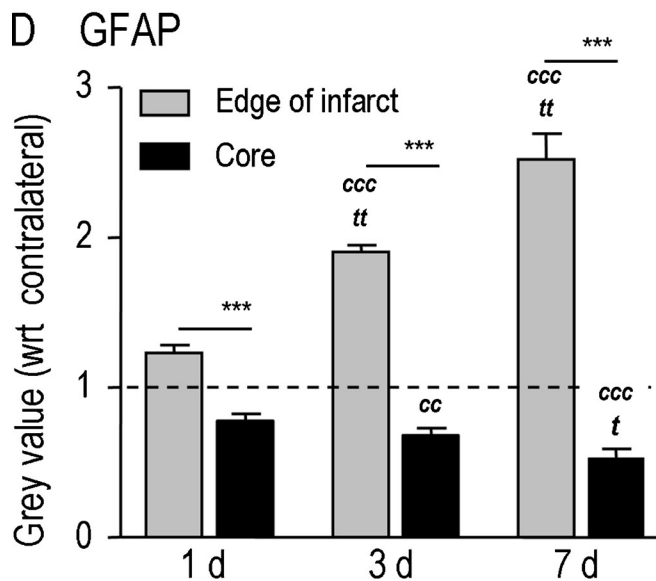
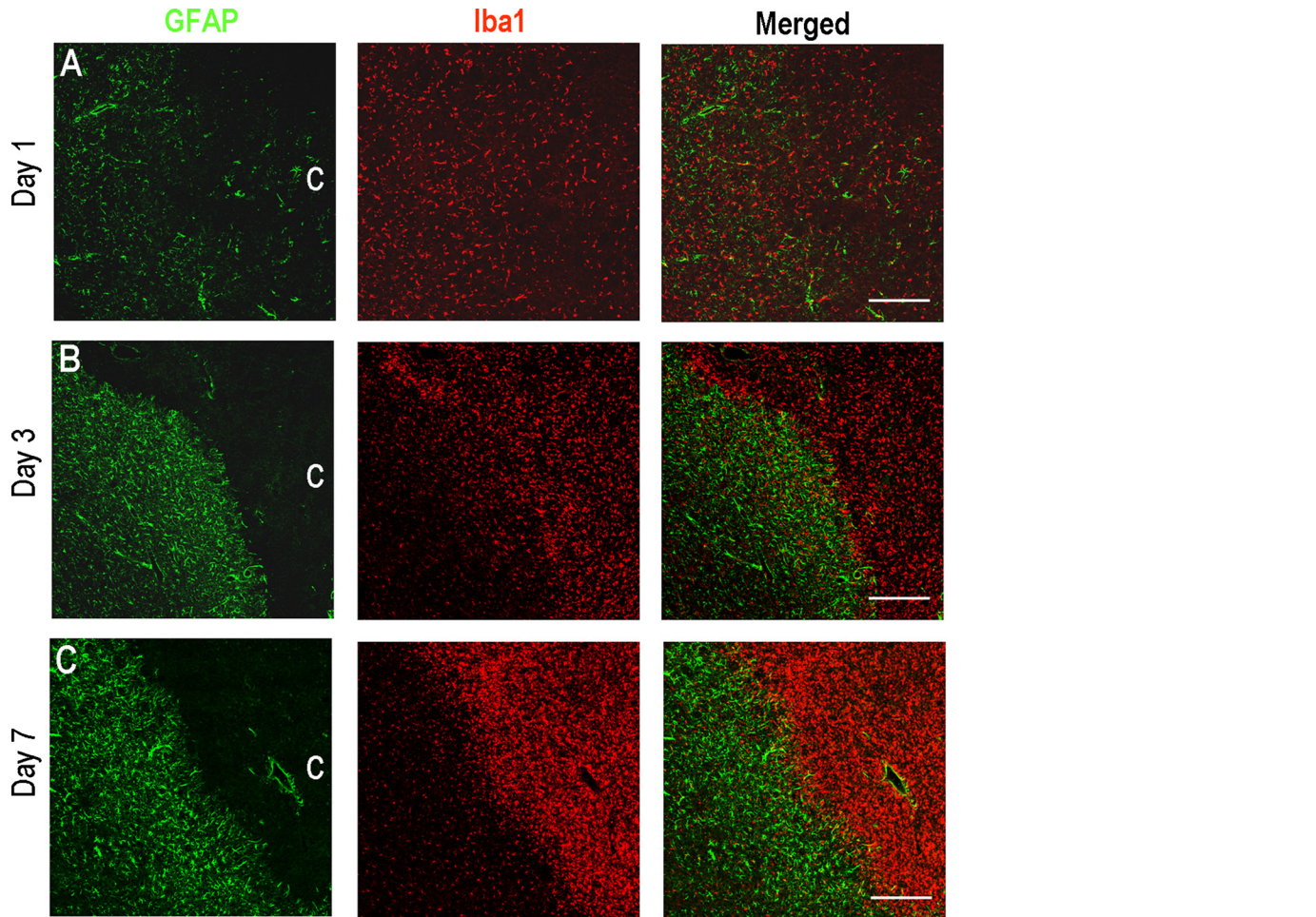


(Fig. 7A). In contrast, most MBP-stained myelinated bundles in both locations were infiltrated with activated microglia/macrophages by Day 3 (Fig. 7B). By Day 7, the core was filled with intensely stained microglia/macrophages (Fig. 7C). Spatial comparisons with myelin could not be made because the bundles no longer stained for MBP, but at the edge of the infarct on Day 7, MBP-stained bundles were surrounded by microglia/macrophages, with apparently fewer inside.

### Detailed Relationship Between Microglia/Macrophages and Myelin Damage

Myelinated tracts in the striatum extend in the rostral-caudal axis, and because the sections were taken every 16  $\mu\text{m}$ , the same tracts could be identified in adjacent MBP-stained serial sections. Hence, correlations of staining with incompatible antibodies from the same host species could be made. First, we monitored MBP and dMBP staining in double-labeled sections at each time point (Fig. 8, left panels). Only Days 3 (Figs. 8A, C) and 7 (Figs. 8B, D) are shown because there was very little damage on Day 1 (Fig. 3). At each time point, an adjacent serial section (middle panels) was double-labeled with anti-MBP and anti-Iba1 to correlate microglia/macrophages with undamaged and damaged myelin bundles. Higher magnification images (right-hand panels) were used to determine the average number of microglia/macrophages in each myelinated bundle (Fig. 8E). In the core on both days (Figs. 8A, B), almost all bundles contained damaged myelin, the density of activated microglia/macrophages increased (also shown in Fig. 6), and they had infiltrated the bundles. The number of microglia/macrophages per myelinated bundle progressively increased from Days 1 to 7 (Fig. 8E).

Spatial and temporal relationships between microglia/macrophages and damaged myelin bundles could also be examined at the infarct edges. For example, on Day 3, both normal and damaged axon bundles were seen in the same image (Fig. 8C). At higher magnification (right panel), it is clear that microglia/macrophages surrounded undamaged bundles (upper image) but had infiltrated the damaged bundles (lower image). Similarly on Day 7, both undamaged and damaged axon bundles were present (Fig. 8D), and microglia/macrophages surrounded the undamaged bundles but had extensively infiltrated the damaged bundles. These observations were corroborated by the quantitative analysis (Fig. 8E). In the core, there were some microglia/macrophages within damaged bundles as early as Day 1, and this number substantially increased on Days 3 and 7. Although microglia/macrophages were seen within axon bundles by Days 3 and 7 at the edge of the infarct, there were significantly more cells within bundles in

the core. No microglia/macrophages were seen in normal myelinated bundles in the undamaged contralateral striatum at any time point.

## DISCUSSION

The salient findings of the present study were as follows.

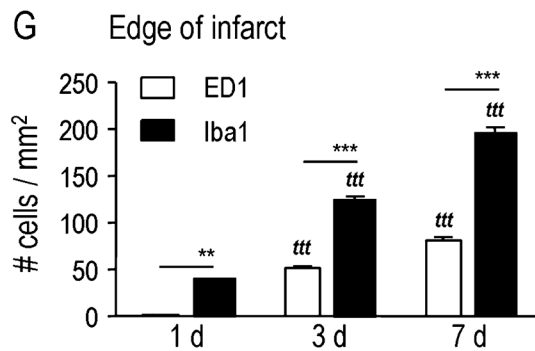
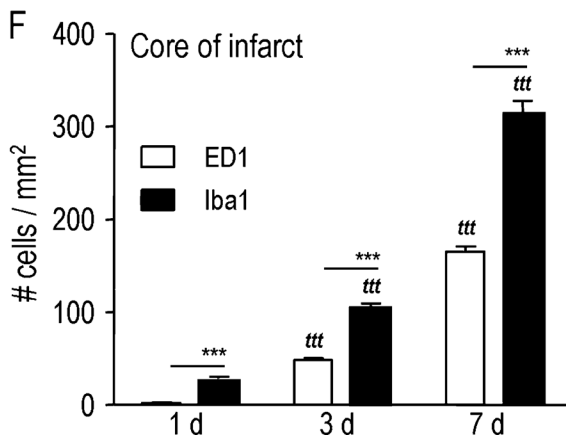
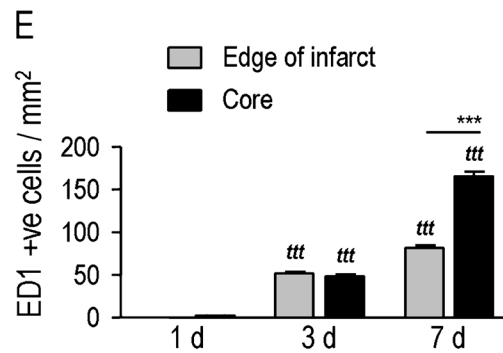
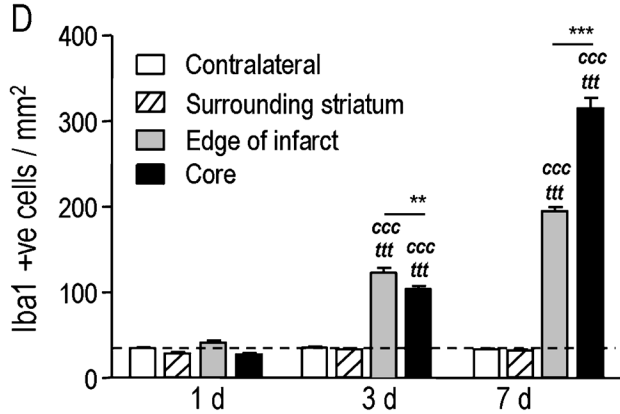
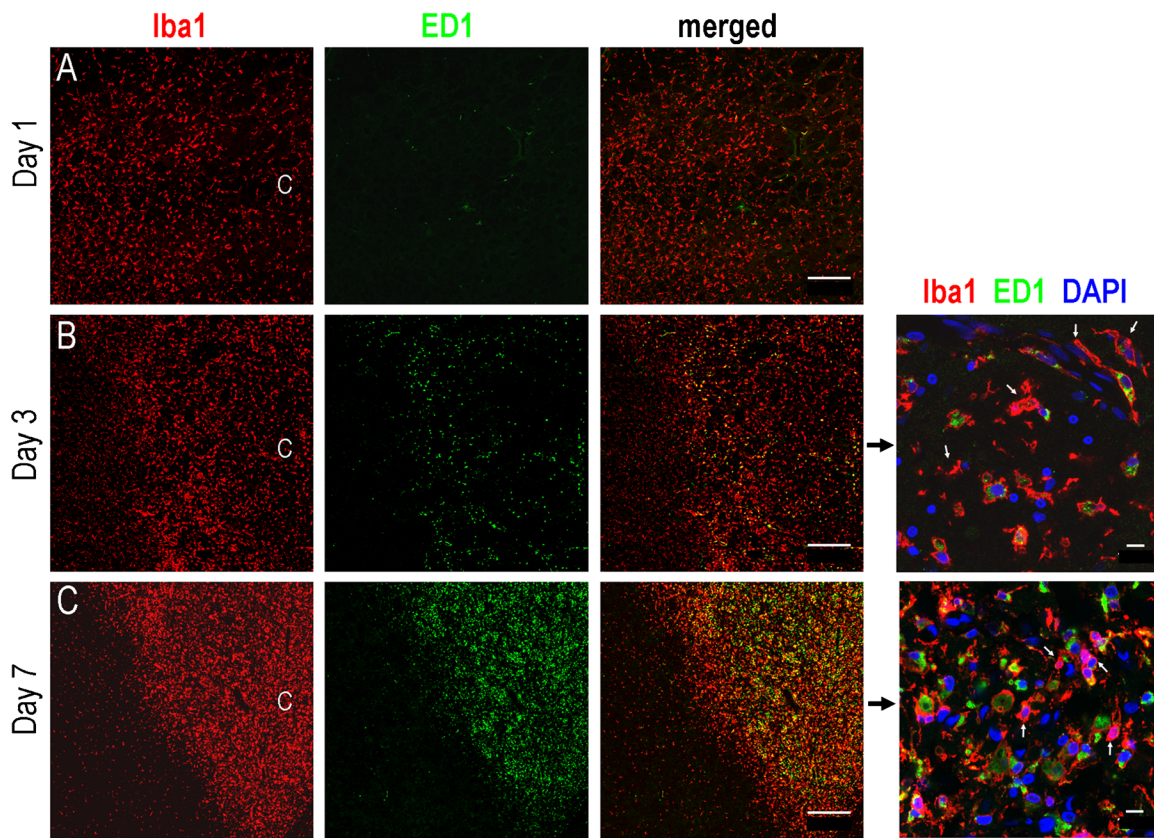
- 1) Neutrophils were present both around and inside myelinated bundles at the earliest time examined (Day 1), their numbers decreased by Day 3, and they were not detected by Day 7.
- 2) The density of activated microglia/macrophages dramatically increased during the 7 days in the core and at the edge of the lesion.
- 3) During the 7-day period examined, the lesion became increasingly demarcated by a glial limitans composed of reactive astrocytes.
- 4) Myelin damage began in the infarct core on Day 1 and then progressed to the edge of the infarct on Days 3 and 7, whereas damage was not seen in more distant striatal tissue surrounding the infarct. Conversely, axonal damage first appeared at the edge of the infarct on Day 1 and then progressed into the core from Days 3 to 7.
- 5) Detailed spatial analyses showed that microglia/macrophages surrounded but did not infiltrate undamaged myelinated bundles, whereas they infiltrated damaged bundles. There were important differences in the spatial and temporal distribution of Iba1 (microglia/macrophage marker) and ED1 staining (lysosomal marker, increased in phagocytic cells). The microglia/macrophages surrounding myelinated bundles were activated, but not phagocytic, whereas phagocytic cells infiltrated bundles in the zone of progressive white matter damage. Our results suggest that neutrophils and microglia/macrophages contribute differently to myelin and axonal injury after ischemic stroke and that there are as yet unknown signals that exclude activated microglia/macrophages from undamaged myelinated bundles but allow them to infiltrate damaged bundles.

### The Endothelin-1 Stroke Model

There are surprisingly few reports on white matter injury after experimental stroke and several discrepancies, even when the same model was used. No animal model fully recapitulates human ischemic stroke. The endothelin-1 model has become popular because it causes reproducible lesions, can target smaller and more specific regions than vessel occlusion models, and does not mechanically damage the cerebral vasculature (5, 21, 24–27, 36). These features were especially important for the present study.

In previous studies, a wide range of endothelin-1 concentrations has been used, with a range of infarct sizes that

**FIGURE 5.** Formation of a glial limitans. **(A–C)** Representative confocal images of double-labeled sections showing astrocytes stained with mouse anti-glial fibrillary acidic protein ([anti-GFAP] green) and rabbit anti-ionized calcium-binding adapter-1 ([anti-Iba1] red) for microglia/macrophages. The damaged ipsilateral striatum at the edge of the infarct is shown at 1, 3, and 7 days after the stroke. The core (c) is to the right in each panel. Scale bars = 400  $\mu\text{m}$ . **(D, E)** Summary of temporal and spatial changes in intensity (normalized to the contralateral striatum; dotted line) and area of staining (expressed as percent of total area examined) from 1 to 7 days after an ischemic stroke. Values are shown as mean  $\pm$  SEM for 4 sampling areas at each location and time (4 rats per time point). Statistical comparisons are based on 2-way analysis of variance with Bonferroni post hoc tests. Levels of significance and comparisons are as follows: *c*, *cc*, *ccc*, different from the contralateral striatum ( $p < 0.05$ ,  $p < 0.01$ ,  $p < 0.001$ , respectively); \*\*\* the core differs from the edge ( $p < 0.001$ ); *t*, *tt*, *ttt*, different from the previous time point at the same site ( $p < 0.05$ ,  $p < 0.01$ ,  $p < 0.001$ , respectively).



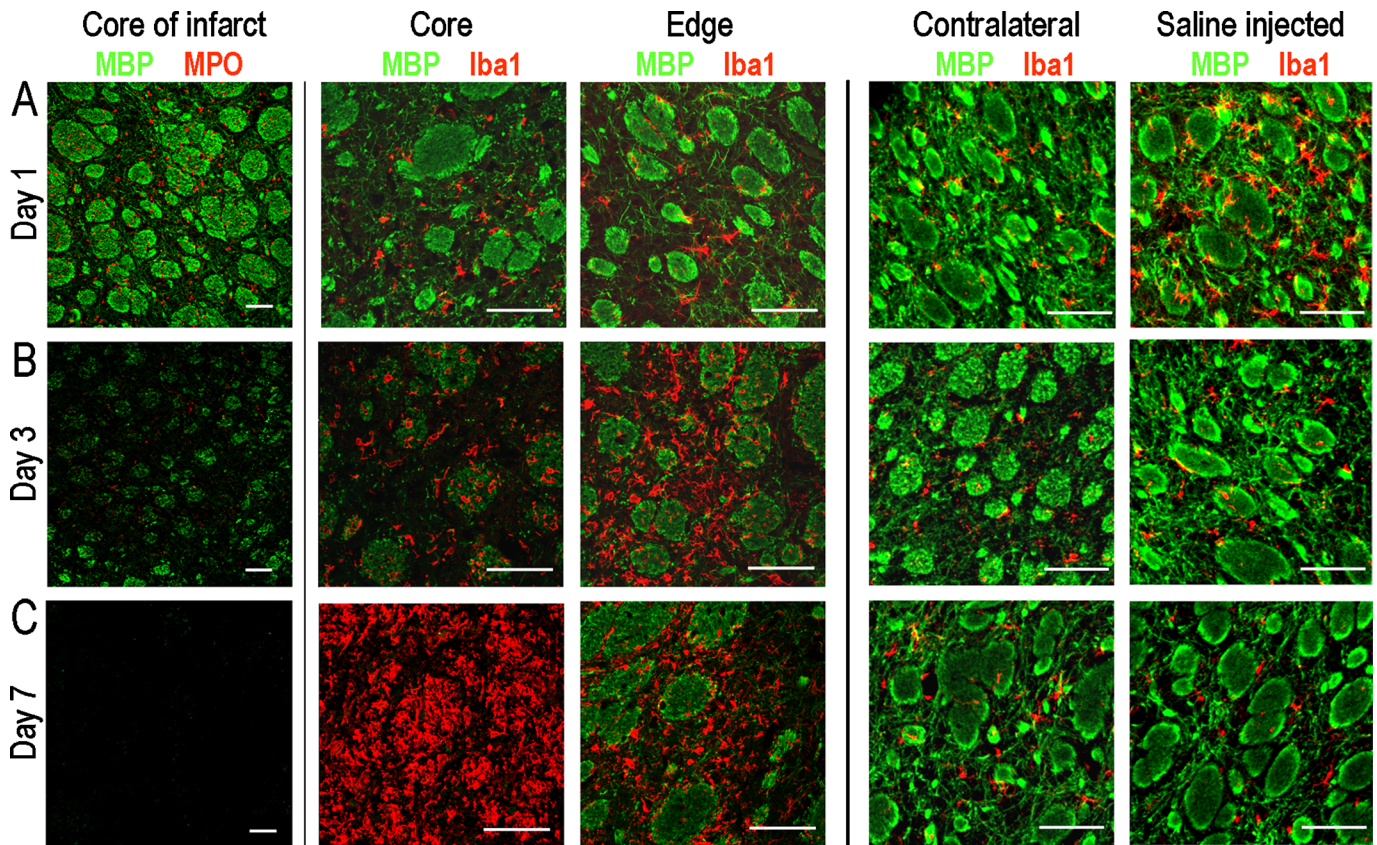
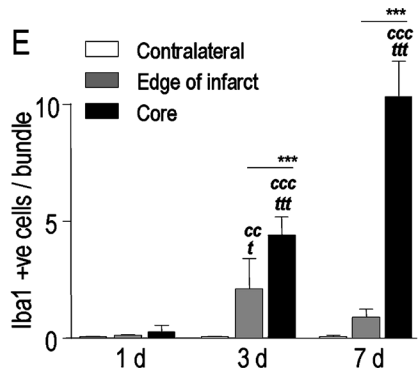
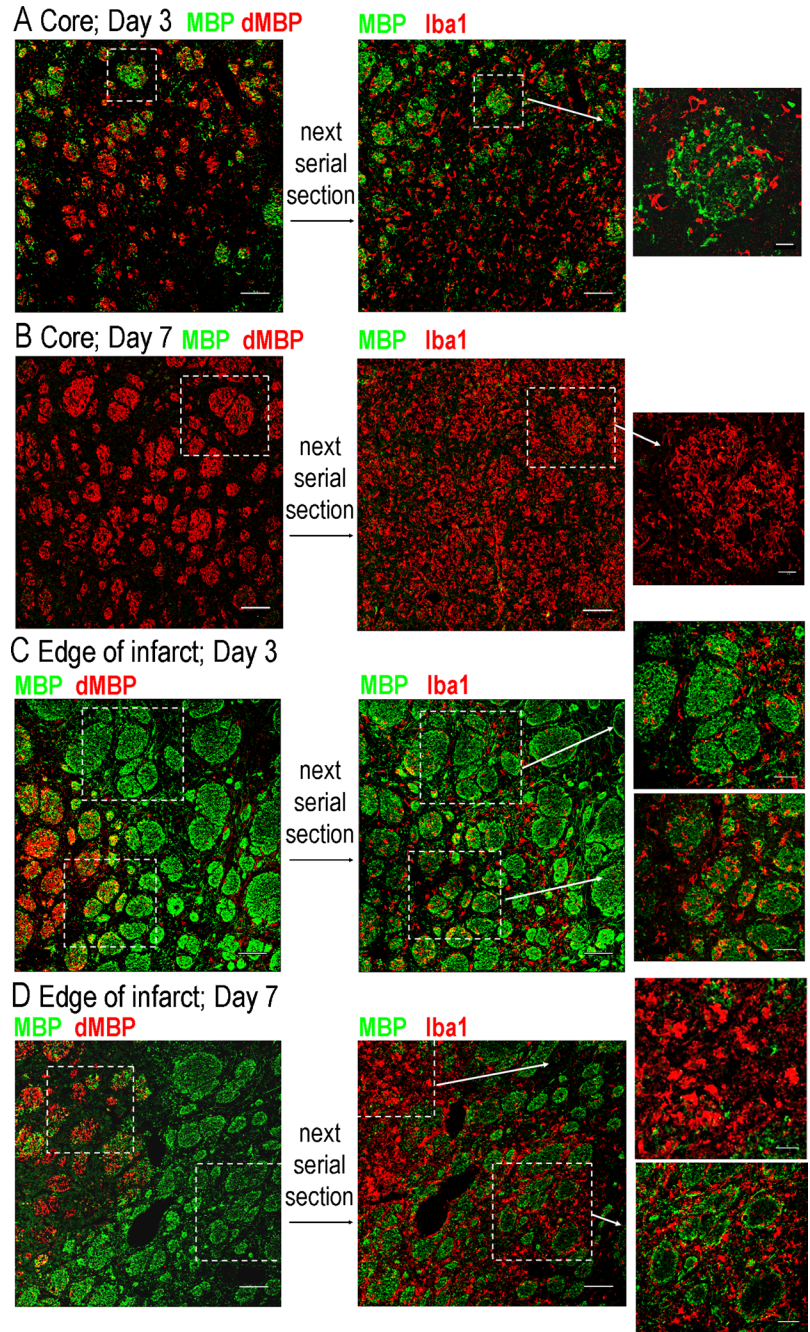


**FIGURE 7.** Spatial and temporal relationships of neutrophils, microglia/macrophages and myelinated bundles. In the left hand panels, at 1 (**A**), 3 (**B**) and 7 days (**C**), neutrophils in the core of the infarct were labeled with rabbit polyclonal antibodies against myeloperoxidase ([MPO] red) and normal myelin basic protein ([MBP] green). Images were taken at a lower magnification to illustrate the extent of neutrophil entry. The remaining panels show double labeling for MBP (green) and microglia/macrophages (ionized calcium-binding adapter-1 [Iba1], red) in the core, at the edge of the infarct (the core is out of view to the left), and in the undamaged contralateral striatum. Myelinated bundles throughout the core and edge of the infarct in (**B**) are infiltrated with microglia/macrophages. The pairs of panels to the right compare the contralateral striatum with saline-injected rats at each time point. Scale bars = 100  $\mu\text{m}$ .

might account for some differing results. It is important to note that activity of this peptide depends on storage conditions and duration, which highlights the need to report lesion size. In the present study, the striatal lesions ( $41 \pm 2 \text{ mm}^3$ ) were about the same size ( $49.4 \text{ mm}^3$ ) as an earlier study using

the same amount of endothelin-1 (400 pmol) (26). In other studies, much smaller lesions ( $\sim 6 \text{ mm}^3$ ) with 430 pmol (24) and much larger lesions ( $75.5 \text{ mm}^3$ ) with 500 pmol (38) are reported. Using an extremely small endothelin-1 dose (10 pmol), 1 study reported intermediate-sized lesions

**FIGURE 6.** Accumulation of activated microglia/macrophages in time and space after ischemic injury. (**A–C**) Representative confocal images of double-labeled sections showing microglia/macrophages labeled with an antibody against ionized calcium-binding adapter-1 ([Iba1] red) and highly activated microglia/macrophages labeled with an antibody against the lysosomal marker, ED1 (green). The damaged ipsilateral striatum at the edge of the infarct is shown at 1, 3, and 7 days after the stroke. The core (marked c) is to the right in each panel. Panels at right show higher magnification images; arrowheads indicate examples of cells stained with Iba1 but not ED1. DAPI was used to label cell nuclei (blue). Scale bars = (main panels) 400  $\mu\text{m}$ ; (higher-magnification panels) 20  $\mu\text{m}$ . (**D–G**) Summary of temporal and spatial changes in density of microglia/macrophages from 1 to 7 days after the stroke. Panel (**D**) compares the density of Iba1-labeled cells in the undamaged contralateral striatum (white bars and dotted line) and the ipsilateral surrounding striatum, with the edge and core of the infarct. Panel (**E**) shows the density of ED1-labeled cells in the core and at the edge of the infarct. No ED1-labeled cells were detected in the contralateral or surrounding ipsilateral striatum (not shown). Panels (**F**) and (**G**) compare the densities of Iba1- and ED1-labeled cells in the core and at the edge of the infarct. Values are shown as mean  $\pm$  SEM for 4 sampling areas at each location and time (4 rats per time point). Statistical comparisons are based on 2-way analysis of variance with Bonferroni post hoc tests. In (**D**), ccc indicates differences from the contralateral striatum ( $p < 0.001$ ). There were no differences between the surrounding striatum and contralateral striatum at any time. The remaining comparisons are: *t*t, different from the previous time point at the same site ( $p < 0.001$ ); \*\*, \*\*\* the core differs from the edge ( $p < 0.01$ ,  $p < 0.001$ , respectively).



(17.5 mm<sup>3</sup>) (5), and another (21) did not show the lesion or report the size.

### Evolution of the White Matter Injury

Most stroke studies have characterized myelin damage as loss of immunoreactivity for MBP (4, 21, 39) or as reduced Luxol fast blue staining (4, 40). By quantifying the change in areas and intensities of staining for both MBP and dMBP, we show myelin damage beginning in the core at 1 day and progressing for at least 7 days. Our recent study is apparently the only stroke-related study that has directly compared antibodies directed against normal and dMBP (41). In that study of intracerebral hemorrhage, we observed progressive myelin damage both inside and at the edge of the hematoma during the first 7 days, much as in the present study. The dMBP antibody has been used to demonstrate demyelination from 1 to 30 days after inducing chronic ischemia (42), and myelin breakdown in the hippocampus after hypoxic-ischemic injury (43). The few existing reports of changes in normal MBP staining after cerebral ischemia differ in their conclusions, but detailed comparisons cannot be made because none quantified the changes or compared different regions of the lesion. Myelin damage was shown only at 1 day (5) or 3 and 7 days (21) after endothelin-1 injection into the striatum, and 1 to 2 weeks after middle cerebral artery occlusion (MCAo) (4).

We also monitored APP, a sensitive marker of axon dysfunction (31). Here, and after intracerebral hemorrhage (41), axon damage was evident by Day 3 at the edge of the infarct and progressed into the core, which supports the view that axon damage can occur in the absence of demyelination. Our results are consistent with earlier studies that showed early APP accumulation around the infarct in the MCAo model (4, 44) or after photochemically induced common carotid artery thrombosis (32). It is possible that differences from other studies are caused by infarct size; in the MCAo model, APP accumulation correlated with lesion volume (44). In the 2 studies in which extremely small amounts of endothelin-1 were injected into the striatum, one produced intermediate-sized lesions and observed APP accumulation (5) and the other saw no accumulation but did not report the lesion size (21).

### Relationship of the Inflammatory Response to White Matter Damage

After acute CNS injury, the lesion becomes surrounded by a glial scar (glial limitans) composed of reactive astrocytes, activated microglia, and macrophages that may contribute to

both damage and lesion resolution (13, 45, 46–48). Potentially beneficial roles include physically confining the damage, producing trophic factors, and removing cellular debris by phagocytosis (18, 49, 50). Some inflammatory products can be directly neurotoxic, however, and thus might exacerbate damage in the stroke penumbra (17, 51, 52). We expect that the outcomes of inflammation will differ with proximity to the infarct and at different times during injury development and resolution; thus, it is essential to conduct a detailed analysis of the spatial and temporal development of the inflammatory response.

In the first week after the stroke, we observed progressive formation of a glial scar, wherein reactive astrocytes surrounded the infarct that transiently contained neutrophils and was increasingly infiltrated with activated microglia/macrophages. Neutrophils were present around and inside damaged myelinated bundles at the earliest time examined (1 day), consistent with initiating the myelin damage, and then became undetectable by 7 days. Neutrophils are expected to cause bystander damage because of the large amounts of inflammatory cytokines, reactive oxygen species, and the matrix metalloproteases they produce (53–55). A microglia/macrophage response has been described in numerous stroke studies (52, 56) and has been proposed to mediate white matter damage (57) but with little evidence. Our quantitative analysis showed that progressive myelin damage coincided in time and space with a large increase in activated microglia/macrophages and not with reactive astrocytes, but also suggests more complex roles for these cells. In the infarct core, both axon and myelin damage progressively worsened during the 7 days, and large numbers of activated microglia/macrophages infiltrated the myelinated bundles; thus, they might initiate and perpetuate the myelin damage at this location. Axon damage began by Day 1 at the edge of the lesion in a zone containing activated microglia/macrophages (not neutrophils) that were appropriately positioned to cause the axon injury. At this early time point, microglia/macrophages had not infiltrated into the myelinated tracts despite the evident axon damage, suggesting that these 2 white matter components are damaged by different mechanisms. During the 7-day period, the density of activated microglia/macrophages increased; they first surrounded undamaged myelinated bundles and later infiltrated only the damaged bundles, which suggests that these cells respond to damage in the myelinated tracts beyond the lesion core.

Many experimental stroke studies have reported rapid but short-lived neutrophil recruitment (34, 35, 58, 59), but there are

**FIGURE 8.** Detailed relationship between microglia/macrophages and myelin damage. Left panels. Representative confocal images of normal myelin (mouse anti-myelin basic protein [anti-MBP], green) and damaged myelin ([anti-dMBP] red). On Days 3 and 7 after the stroke, double-labeled sections are shown for the core (**A, B**) and the edge of the infarct (**C, D**) the core is out of view to the left). Scale bars = 100  $\mu$ m. Middle panels: Adjacent serial sections were double stained for normal myelin ([MBP] green) and microglia/macrophages using anti-ionized calcium-binding adapter-1 ([Iba1 antibody] red). The boxes in the left and middle panels indicate the same myelinated bundles in adjacent serial sections. Scale bars = 100  $\mu$ m. Right panels: Higher-magnification images of the boxed regions in the middle panels. Scale bars = (top 2 panels) 15  $\mu$ m; (lower 4 panels) 50  $\mu$ m. (**E**) Summary of the number of microglia/macrophages per axon bundle. The Iba1-labeled cells located inside MBP- or dMBP-labeled bundles were manually counted in a 369  $\times$  369- $\mu$ m sampling area each in the core, edge of the infarct, and the contralateral striatum. Values are shown as mean  $\pm$  SD for 4 rats at each time point. Statistical comparisons are based on 2-way analysis of variance with Bonferroni post hoc tests: *cc*, *ccc*, differences from the contralateral striatum ( $p < 0.01$ ,  $p < 0.001$ , respectively); \*\*\* the core differs from the edge ( $p < 0.001$ ); *t*, *ttt*, different from the previous time point at the same site ( $p < 0.05$ ,  $p < 0.001$ , respectively).

discrepancies in the timing and in the reported accumulation of activated microglia and macrophages. In 3 previous studies of neutrophils using the endothelin-1 model, 1 study observed peak neutrophil numbers at 1 day, which decreased at 3 days and were undetectable by 7 days (21). Another study reported a complete absence of neutrophils (5), and a recent study reported neutrophils as early as Day 1 but showed that approximately 50% of them were inside “macrophages” by Day 3 (36). The reasons for these discrepancies are not clear but might reflect the labeling methods. We labeled neutrophils with an antibody against myeloperoxidase and saw no difference whether a sodium citrate antigen retrieval technique was used. Two articles used antibodies against unknown neutrophil antigens, that is, HB199 without antigen retrieval (5) and MBS-1 with antigen retrieval (21).

To assess inflammation, previous studies of white matter damage after ischemic stroke have used the ED1 antibody to label cells they call *macrophages*, apparently ignoring the contribution of resident microglia. ED1 is not a comprehensive marker for activated microglia/macrophages, it predominantly labels lysosomes and is increased when these cells become phagocytic (60). Using the endothelin-1 model of striatal stroke, 1 report showed no recruitment of ED1-labeled cells until Day 3 (5), whereas another saw accumulation at Day 1 with maximal accumulation at 3 and 7 days (21). Axonal damage was not observed in either study. One study using the MCAo stroke model reported an increase in Iba1 staining, but no ED1 staining in the peri-ischemic area at 7 days (61), implying a lack of phagocytosis in the penumbra. We detected ED1 staining beginning at 3 days postinjury, and more Iba1-labeled microglia/macrophages became ED1 positive in the core than at the edge of the infarct. About 50% were double labeled at 3 and 7 days in both locations. The brightly stained Iba1-positive cells surrounding intact myelinated bundles in the penumbra had an activated morphology (i.e. retracted processes) but did not stain for ED1 and, thus, were not likely phagocytic. In contrast, ED1-labeled cells (presumably phagocytes) were present in the zone of progressive white matter damage. This differential pattern of staining supports our hypothesis that microglia/macrophages perform different functions within and outside the core, which cannot be deduced from their “activated” morphology alone. In the future, it will be valuable to assess molecular states of microglia/macrophage activation and their products with time and location after the stroke.

This study provides the first such quantification of temporal and spatial relationships between inflammation and white matter damage after experimental stroke and should provide a useful framework for future work on potential therapeutic interventions.

#### ACKNOWLEDGMENTS

*The authors thank Dr Jason K. Wasserman (a former PhD candidate in Schlichter Laboratory) for numerous helpful discussions about the project and results and for initially instructing Iska Moxon-Emre in surgical and immunohistochemical techniques. The authors also thank Dr S. Lively (Schlichter Laboratory) for providing Figure 1B, and Helen Yang and Adina Diaconescu for technical contributions in the early stages of this work.*

#### REFERENCES

- Lo EH, Dalkara T, Moskowitz MA. Mechanisms, challenges and opportunities in stroke. *Nat Rev Neurosci* 2003;4:399–415
- Lopez AD, Mathers CD, Ezzati M, et al. Global and regional burden of disease and risk factors, 2001: Systematic analysis of population health data. *Lancet* 2006;367:1747–57
- Petty MA, Wettstein JG. White matter ischaemia. *Brain Res Brain Res Rev* 1999;31:58–64
- Irving EA, Bentley DL, Parsons AA. Assessment of white matter injury following prolonged focal cerebral ischaemia in the rat. *Acta Neuropathol* 2001;102:627–35
- Hughes PM, Anthony DC, Ruddin M, et al. Focal lesions in the rat central nervous system induced by endothelin-1. *J Neuropathol Exp Neurol* 2003;62:1276–86
- Dewar D, Yam P, McCulloch J. Drug development for stroke: Importance of protecting cerebral white matter. *Eur J Pharmacol* 1999;375:41–50
- Medana IM, Esiri MM. Axonal damage: A key predictor of outcome in human CNS diseases. *Brain* 2003;126:515–30
- Matute C, Alberdi E, Domercq M, et al. Excitotoxic damage to white matter. *J Anat* 2007;210:693–702
- Astrup J, Siesjo BK, Symon L. Thresholds in cerebral ischemia—the ischemic penumbra. *Stroke* 1981;12:723–25
- Bullock R, Brock-Utne J, van Dellen J, et al. Intracerebral hemorrhage in a primate model: Effect on regional cerebral blood flow. *Surg Neurol* 1988;29:101–7
- Du C, Hu R, Csernansky CA, et al. Very delayed infarction after mild focal cerebral ischemia: A role for apoptosis? *J Cereb Blood Flow Metab* 1996;16:195–201
- Endres M, Namura S, Shimizu-Sasamata M, et al. Attenuation of delayed neuronal death after mild focal ischemia in mice by inhibition of the caspase family. *J Cereb Blood Flow Metab* 1998;18:238–47
- Zhang W, Stanimirovic D. Current and future therapeutic strategies to target inflammation in stroke. *Curr Drug Targets Inflamm Allergy* 2002;1:151–66
- Kochanek PM, Hallenbeck JM. Polymorphonuclear leukocytes and monocytes/macrophages in the pathogenesis of cerebral ischemia and stroke. *Stroke* 1992;23:1367–79
- Emsley HC, Tyrrell PJ. Inflammation and infection in clinical stroke. *J Cereb Blood Flow Metab* 2002;22:1399–419
- Bramlett HM, Dietrich WD. Pathophysiology of cerebral ischemia and brain trauma: Similarities and differences. *J Cereb Blood Flow Metab* 2004;24:133–50
- Stoll G, Jander S, Schroeter M. Detrimental and beneficial effects of injury-induced inflammation and cytokine expression in the nervous system. *Adv Exp Med Biol* 2002;513:87–113
- Schwartz M. Macrophages and microglia in central nervous system injury: Are they helpful or harmful? *J Cereb Blood Flow Metab* 2003;23:385–94
- Hailer NP. Immunosuppression after traumatic or ischemic CNS damage: It is neuroprotective and illuminates the role of microglial cells. *Prog Neurobiol* 2008;84:211–33
- Coleman MP, Perry VH. Axon pathology in neurological disease: A neglected therapeutic target. *Trends Neurosci* 2002;25:532–37
- Souza-Rodrigues RD, Costa AM, Lima RR, et al. Inflammatory response and white matter damage after microinjections of endothelin-1 into the rat striatum. *Brain Res* 2008;1200:78–88
- Sudlow CL, Warlow CP. Comparable studies of the incidence of stroke and its pathological types: Results from an international collaboration. *International Stroke Incidence Collaboration. Stroke* 1997;28:491–99
- Bamford JM, Warlow CP. Evolution and testing of the lacunar hypothesis. *Stroke* 1988;19:1074–82
- Fuxe K, Kurosawa N, Cintra A, et al. Involvement of local ischemia in endothelin-1 induced lesions of the neostriatum of the anesthetized rat. *Exp Brain Res* 1992;88:131–39
- Frost SB, Barbay S, Mumert ML, et al. An animal model of capsular infarct: Endothelin-1 injections in the rat. *Behav Brain Res* 2006;169:206–11
- Windle V, Szymanska A, Granter-Button S, et al. An analysis of four different methods of producing focal cerebral ischemia with endothelin-1 in the rat. *Exp Neurol* 2006;201:324–34

27. Sharkey J, Butcher SP. Characterisation of an experimental model of stroke produced by intracerebral microinjection of endothelin-1 adjacent to the rat middle cerebral artery. *J Neurosci Methods* 1995;60:125–31
28. Matsuo A, Lee GC, Terai K, et al. Unmasking of an unusual myelin basic protein epitope during the process of myelin degeneration in humans: A potential mechanism for the generation of autoantigens. *Am J Pathol* 1997;150:1253–66
29. Eng LF, Ghirmikar RS, Lee YL. Glial fibrillary acidic protein: GFAP-thirty-one years (1969–2000). *Neurochem Res* 2000;25:1439–51
30. Gentleman SM, Nash MJ, Sweeting CJ, et al. Beta-amyloid precursor protein (beta APP) as a marker for axonal injury after head injury. *Neurosci Lett* 1993;160:139–44
31. Thinakaran G, Koo EH. Amyloid precursor protein trafficking, processing, and function. *J Biol Chem* 2008;283:29615–19
32. Dietrich WD, Kraydieh S, Prado R, et al. White matter alterations following thromboembolic stroke: A beta-amyloid precursor protein immunocytochemical study in rats. *Acta Neuropathol* 1998;95:524–31
33. Streit WJ, Walter SA, Pennell NA. Reactive microgliosis. *Prog Neurobiol* 1999;57:563–81
34. Barone FC, Feuerstein GZ. Inflammatory mediators and stroke: New opportunities for novel therapeutics. *J Cereb Blood Flow Metab* 1999;19:819–34
35. Emerich DF, Dean RL 3rd, Bartus RT. The role of leukocytes following cerebral ischemia: Pathogenic variable or bystander reaction to emerging infarct? *Exp Neurol* 2002;173:168–81
36. Weston RM, Jones NM, Jarrott B, et al. Inflammatory cell infiltration after endothelin-1-induced cerebral ischemia: Histochemical and myeloperoxidase correlation with temporal changes in brain injury. *J Cereb Blood Flow Metab* 2007;27:100–14
37. Ito D, Imai Y, Ohsawa K, et al. Microglia-specific localisation of a novel calcium binding protein, Iba1. *Brain Res Mol Brain Res* 1998;57:1–9
38. Bogaert L, Scheller D, Moonen J, et al. Neurochemical changes and laser Doppler flowmetry in the endothelin-1 rat model for focal cerebral ischemia. *Brain Res* 2000;887:266–75
39. Biran V, Joly LM, Heron A, et al. Glial activation in white matter following ischemia in the neonatal P7 rat brain. *Exp Neurol* 2006;199:103–12
40. Schabitz WR, Li F, Fisher M. The N-methyl-D-aspartate antagonist CNS 1102 protects cerebral gray and white matter from ischemic injury following temporary focal ischemia in rats. *Stroke* 2000;31:1709–14
41. Wasserman JK, Schlichter LC. White matter injury in young and aged rats after intracerebral hemorrhage. *Exp Neurol* 2008;214:266–75
42. Wakita H, Tomimoto H, Akiguchi I, et al. Axonal damage and demyelination in the white matter after chronic cerebral hypoperfusion in the rat. *Brain Res* 2002;924:63–70
43. Rao R, Tkac I, Townsend EL, et al. Perinatal iron deficiency predisposes the developing rat hippocampus to greater injury from mild to moderate hypoxia-ischemia. *J Cereb Blood Flow Metab* 2007;27:729–40
44. Yam PS, Takasago T, Dewar D, et al. Amyloid precursor protein accumulates in white matter at the margin of a focal ischaemic lesion. *Brain Res* 1997;760:150–57
45. Barone FC, Irving EA, Ray AM, et al. Inhibition of p38 mitogen-activated protein kinase provides neuroprotection in cerebral focal ischemia. *Med Res Rev* 2001;21:129–45
46. Xie Z, Wei M, Morgan TE, et al. Peroxynitrite mediates neurotoxicity of amyloid  $\beta$ -peptide<sub>1–42</sub> and lipopolysaccharide-activated microglia. *J Neurosci* 2002;22:3484–92
47. Trendelenburg G, Dimagl U. Neuroprotective role of astrocytes in cerebral ischemia: Focus on ischemic preconditioning. *Glia* 2005;50:307–20
48. Rolls A, Shechter R, Schwartz M. The bright side of the glial scar in CNS repair. *Nat Rev Neurosci* 2009;10:235–41
49. Anderson MF, Blomstrand F, Blomstrand C, et al. Astrocytes and stroke: Networking for survival? *Neurochem Res* 2003;28:293–305
50. Turrin NP, Rivest S. Molecular and cellular immune mediators of neuroprotection. *Mol Neurobiol* 2006;34:221–42
51. del Zoppo G, Ginis I, Hallenbeck JM, et al. Inflammation and stroke: Putative role for cytokines, adhesion molecules and iNOS in brain response to ischemia. *Brain Pathol* 2000;10:95–112
52. Wang Q, Tang XN, Yenari MA. The inflammatory response in stroke. *J Neuroimmunol* 2007;184:53–68
53. Justicia C, Panes J, Sole S, et al. Neutrophil infiltration increases matrix metalloproteinase-9 in the ischemic brain after occlusion/reperfusion of the middle cerebral artery in rats. *J Cereb Blood Flow Metab* 2003;23:1430–40
54. Nguyen HX, O'Barr TJ, Anderson AJ. Polymorphonuclear leukocytes promote neurotoxicity through release of matrix metalloproteinases, reactive oxygen species, and TNF- $\alpha$ . *J Neurochem* 2007;102:900–12
55. Wasserman JK, Schlichter LC. Minocycline protects the blood-brain barrier and reduces edema following intracerebral hemorrhage in the rat. *Exp Neurol* 2007;207:227–37
56. Zheng Z, Yenari MA. Post-ischemic inflammation: Molecular mechanisms and therapeutic implications. *Neurol Res* 2004;26:884–92
57. Popovich PG, Guan Z, McGaughy V, et al. The neuropathological and behavioral consequences of intraspinal microglial/macrophage activation. *J Neuropathol Exp Neurol* 2002;61:623–33
58. Clark RK, Lee EV, Fish CJ, et al. Development of tissue damage, inflammation and resolution following stroke: An immunohistochemical and quantitative planimetric study. *Brain Res Bull* 1993;31:565–72
59. Zhang RL, Chopp M, Chen H, et al. Temporal profile of ischemic tissue damage, neutrophil response, and vascular plugging following permanent and transient (2H) middle cerebral artery occlusion in the rat. *J Neurol Sci* 1994;125:3–10
60. Damoiseaux JG, Dopp EA, Calame W, et al. Rat macrophage lysosomal membrane antigen recognized by monoclonal antibody ED1. *Immunology* 1994;83:140–47
61. Ito D, Tanaka K, Suzuki S, et al. Enhanced expression of Iba1, ionized calcium-binding adapter molecule 1, after transient focal cerebral ischemia in rat brain. *Stroke* 2001;32:1208–15